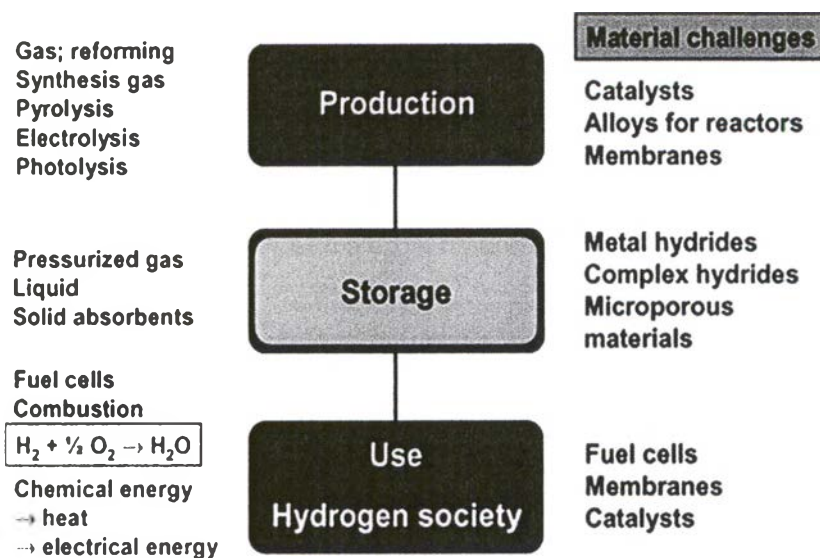


## CHAPTER II LITERATURE SURVEY

### 2.1 Fundamentals of Hydrogen

Hydrogen gas is diatomic (its molecules contain two atoms) at room temperature, but it dissociates into free atoms at high temperatures. The melting point is  $-259.2^{\circ}\text{C}$  and the boiling point is  $-252.7^{\circ}\text{C}$ . The atomic weight of hydrogen gas is  $1.00797\text{ g mol}^{-1}$  with volumetric density of  $0.089\text{ g l}^{-1}$  at  $0^{\circ}\text{C}$  ([http://www.fuelcellstore.com/information/hydrogen\\_safety.html](http://www.fuelcellstore.com/information/hydrogen_safety.html)).

Figure 2.1 simplifies three steps and their current technologies for hydrogen economy. Detailed information will be explained thereafter.



**Figure 2.1** Simplified three steps and current technologies for hydrogen economy ([http://www.funmat.uio.no/Uorganisk/research\\_topics/hydrogen\\_storage\\_a.html](http://www.funmat.uio.no/Uorganisk/research_topics/hydrogen_storage_a.html)).

Figure 2.2 shows the cycle of hydrogen. The process starts from splitting water into hydrogen and oxygen by the process of electrolysis, using electricity generated from renewable energy sources (i.e. the sun). Oxygen is released into the atmosphere, whilst hydrogen is stored and transported. Oxygen from the atmosphere is re-combined with the stored hydrogen in a fuel cell, producing energy and water

vapor. The water vapor is released back into the environment, where it can become part of the cycle once again (<http://www.imr.salford.ac.uk/hytrain/about/why.html>).

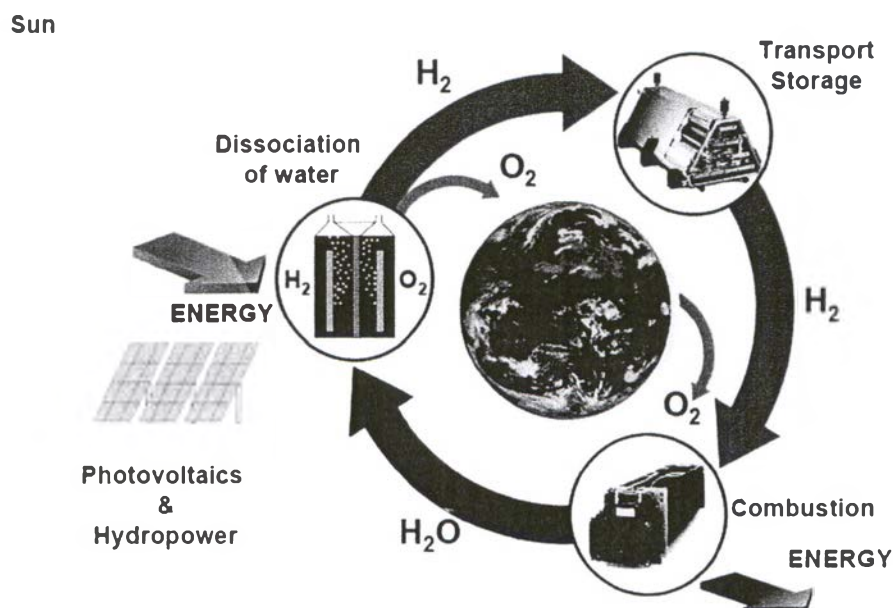


**Figure 2.2** Hydrogen cycle (<http://www.unifr.ch/physics/fk>).

## 2.2 Hydrogen Production

Hydrogen can be produced from renewable energies such as biomass via gasification reaction, direct splitting water by electrolysis reaction that uses energy from photovoltaic solar (PV), wind, or geo-thermal and from fossil fuels namely coal, oil, and natural gas are cracked and/or reformed to hydrogen. Finally, produced hydrogen is sent to storage systems. Figure 2.3 shows a schematic diagram for hydrogen production pathways.

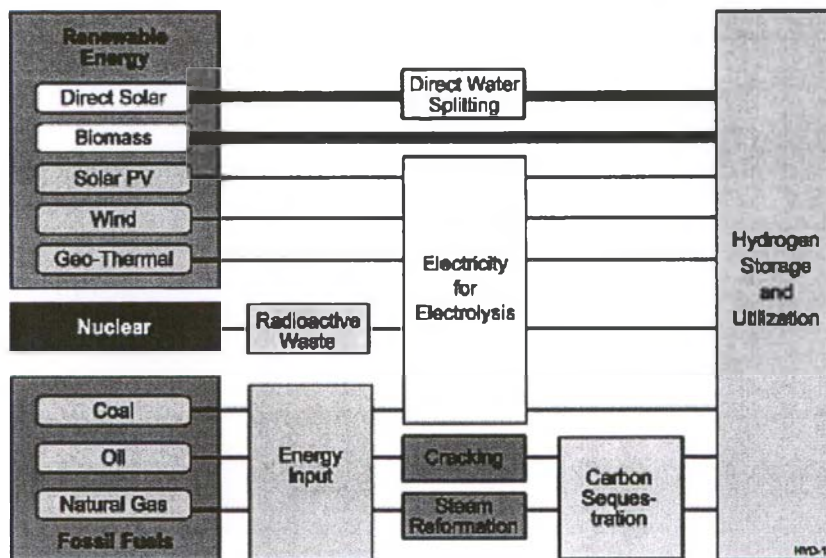
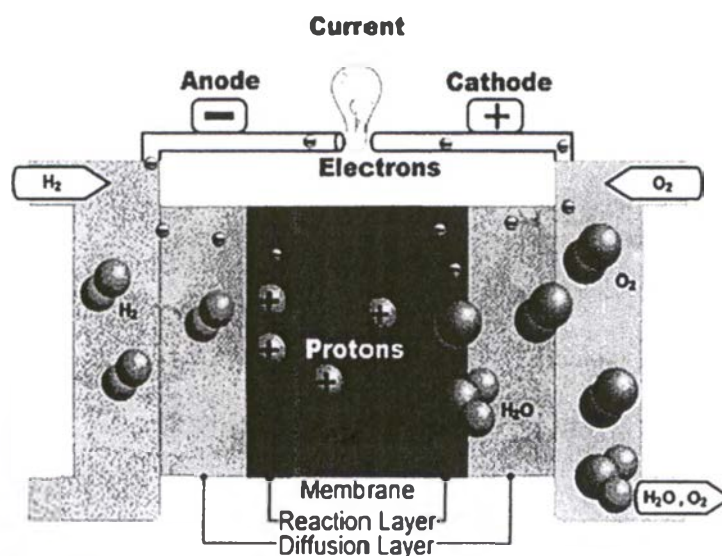


Figure 2.3 Hydrogen production pathways (<http://www.setaram.com>).

### 2.3 Fuel Cells

According to Figure 2.1, one of the goals for the hydrogen storage development is for fuel cells as an energy source. The fuel cells can be used for various applications, including portable, stationary, and transportation systems. All are different and may use different types of fuel cells (<http://www.rpifuelcell.eventurestudio.com/optional/index.cfm>).

In general principle, a fuel cell consists of two electrodes sandwiched around an electrolyte. Oxygen passes over one electrode and hydrogen over the other, generating electricity, water and heat. The hydrogen fuel, from storage systems, is fed into anode of the fuel cell. The oxygen or air enters the fuel cell through cathode. With a suitable catalyst, the hydrogen atom splits into a proton and an electron, which take different paths to the cathode. The proton passes through the electrolyte. The electrons create a separate current that can be utilized before they return to the cathode, to be reunited with the hydrogen and oxygen in a molecule of water. Figure 2.4 gives a better explanation of the fuel cell operation.



**Figure 2.4** Illustration of the PEM fuel cell operation  
([www.esru.strath.ac.uk/EandE/Web\\_sites/00-01/fuel\\_cells/fuel\\_cell\\_operation.html](http://www.esru.strath.ac.uk/EandE/Web_sites/00-01/fuel_cells/fuel_cell_operation.html)).

## 2.4 Hydrogen Storage

Hydrogen is an attractive energy carrier because of its abundance in the environment, zero  $CO_2$  emission, and high energy to mass ratio. However, practical high density storage has been a major barrier to achievement. The hydrogen storage development must be based on the US Department of Energy (DOE) targets in 2015 as follows ([http://www1.eere.energy.gov/hydrogenandfuelcells/storage/pdfs/targets\\_onboard\\_hydro\\_storage\\_explanation.pdf](http://www1.eere.energy.gov/hydrogenandfuelcells/storage/pdfs/targets_onboard_hydro_storage_explanation.pdf)):

- System gravimetric density: 5.5 wt%,
- System volumetric density: 40.0 g l<sup>-1</sup>,
- Fill time for 5 kg fill: 3.3 min,
- Operating temperature: 60 to 120°C.

The hydrogen storage technologies include high-pressure hydrogen, liquid hydrogen, and solid-state hydrogen (including carbon and other high surface area materials,  $H_2O$ -reactive chemical hydrides, thermal chemical hydrides, and

rechargeable metal hydrides) (Riis, 2006). The maximum properties for each technology are shown in Table 2.1. Figure 2.5 compares the volumetric and gravimetric hydrogen density of some of rechargeable metal hydrides.

**Table 2.1** Summary of the hydrogen storage techniques (Züttel, 2004)

Techniques	Volumetric hydrogen density (kgH <sub>2</sub> m <sup>-3</sup> )	Gravimetric hydrogen density (wt %)	Pressure (bar)	Temperature (K)
High-pressure hydrogen	Max 33	13	800	298
Liquid hydrogen	71	100	1	21
Porous solid	Max 150	2	1	298
Metal hydrides	20	4	70	65
Complex hydrides	150	18	1	298
Chemical hydrides	>100	14	1	298

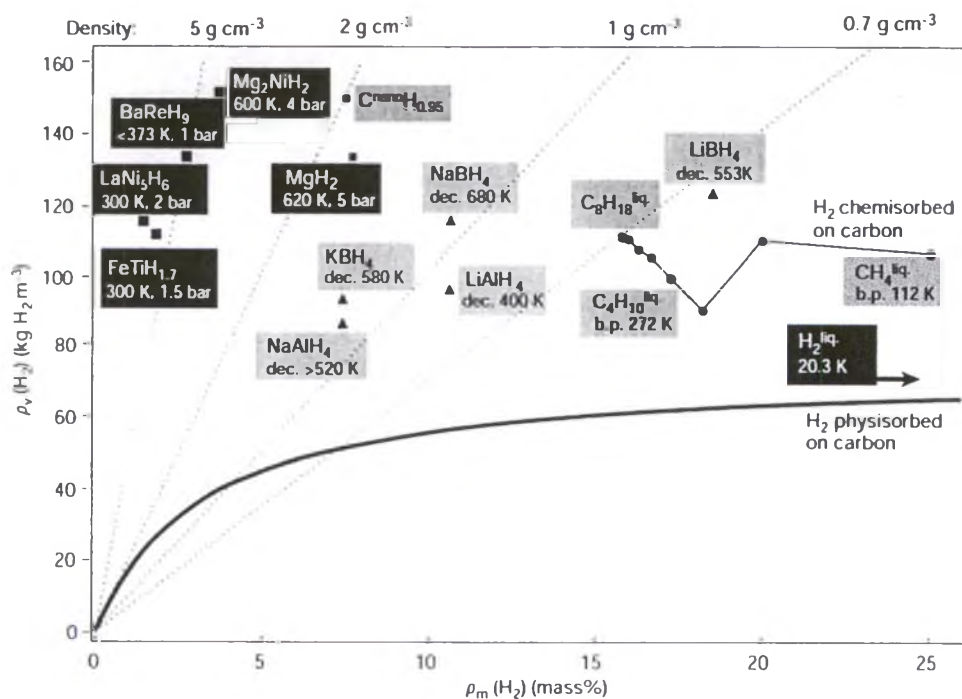


**Figure 2.5** Comparison of the volumetric and gravimetric hydrogen density of metal hydrides, carbon nanotubes, and other hydrocarbons (Schlapbach and Züttel, 2001).

#### 2.4.1 High-pressure Hydrogen Gas Tank

The most commonly used and simplest method is to store hydrogen in its natural form as a gas. Storage of gaseous hydrogen is primarily limited by volume considerations as a result of hydrogen's low density. Even at a high-pressure, very large volumes are required resulting in high material costs. Today gaseous hydrogen is stored at a pressure greater than 50 MPa and with the goal set to 70 MPa or even higher at an ambient temperature (Schlapbach and Züttel, 2001). The most common and conventional steel gaseous cylinders contain a volume of 40 liters and a pressure of 150 bar. Nowadays, fiber-reinforced composite materials are being developed.

#### 2.4.2 Liquid Hydrogen Storage

Hydrogen stored in a liquid form is substantially more compressed than in a gaseous form and superficially it appears an appealing means of energy storage but there are various contributory negative factors. The liquidification requires a large expenditure of energy and liquid hydrogen must be maintained at a

low temperature ( $< 20$  K, the boiling point of hydrogen). There are risks due to the high expansion ratio of liquid hydrogen to gaseous hydrogen. If there is a warming of liquid hydrogen, extremely high pressures could accumulate and result in damage or an explosion. The heat transfer through the container due to boil-off and 30% of energy is loss while the refrigeration process (Ross, 2006).

### 2.4.3 Solid-state Hydrogen

This method includes carbon and other high surface area materials,  $H_2O$ -reactive chemical hydrides, thermal chemical hydrides, and rechargeable metal hydrides (Riis, 2006). Table 2.2 summarizes the potential materials within each of these groups and the details are provided below.

**Table 2.2** Overview of solid hydrogen storage (Riis, 2006)

Carbon and other high surface area material	Chemical hydride ( $H_2O$ -reactive or hydrolysis)
<ul style="list-style-type: none"> <li>• Activated charcoals</li> <li>• Nanotubes</li> <li>• Graphite nanofibers</li> <li>• MOFs, Zeolites, etc.</li> <li>• Clathrate hydrates</li> </ul>	<ul style="list-style-type: none"> <li>• Encapsulated NaH</li> <li>• LiH and <math>MgH_2</math> slurries</li> <li>• <math>CaH_2</math>, <math>LiAlH_4</math>, etc.</li> </ul>
Chemical hydrides (thermal decomposition)	Rechargeable metal hydrides
<ul style="list-style-type: none"> <li>• Ammonia borane</li> <li>• Aluminum hydride</li> </ul>	<ul style="list-style-type: none"> <li>• Alloys and intermetallics</li> <li>• Nanocrystalline</li> <li>• Complex hydrides</li> </ul>

#### 2.4.3.1 *Carbon and Other High Surface Area Materials*

Another method for storing hydrogen is to adsorb molecular hydrogen on a solid with a high surface area, as in a typical molecular sieve. A major mechanism for hydrogen storage is physical or chemical adsorption of hydrogen

either as molecules or as atoms onto a material's surface. It is believed that the enhancement of storage capacity can be achieved with an increase in a surface area (Shi and Hwang, 2007). The materials in the group are carbon nanotubes, activated charcoals, graphite nanofibers, MOFs, zeolite, and clathrate hydrates. The details of some materials are provided below.

(i) Carbon Nanotubes (CNTs)

CNTs are allotropes of carbon with a cylindrical nanostructure. CNTs have been constructed with a diameter on the nanometer scale and a length of tens of microns. They are composed of  $sp^2$  bonds, similar to those observed in graphite and they naturally align themselves into ropes held together by van der Waals forces. CNTs are cylindrical carbon molecules with novel properties. They can be categorized as single-walled nanotubes (SWNTs) and multi-walled nanotubes (MWNTs) (Figure 2.6) (Seetharamappa *et al.*, 2006).

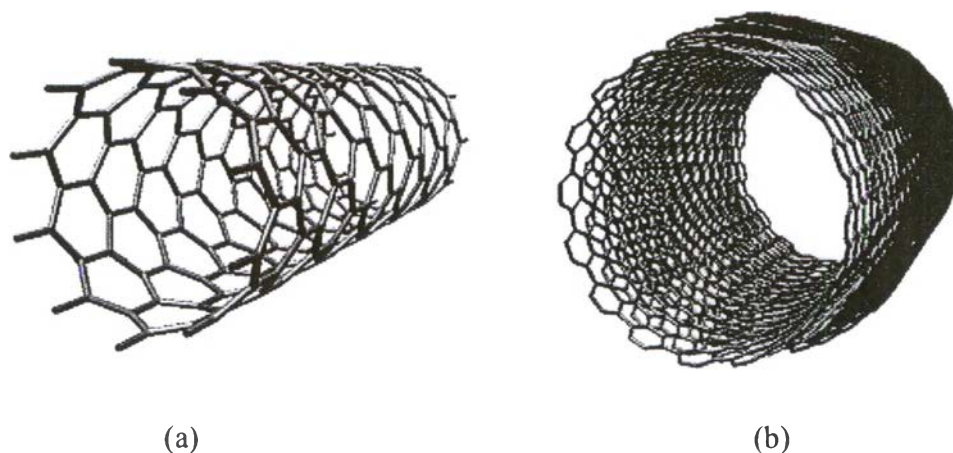


**Figure 2.6** Two types of carbon nanotubes (a) single-walled nanotubes (SWNTs) and (b) multi-walled nanotubes (MWNTs)

([http://www.science.uwaterloo.ca/~foldvari/research\\_program/index.html](http://www.science.uwaterloo.ca/~foldvari/research_program/index.html)).

(ii) Graphite

Graphite is one of the standard forms of carbon. The atoms are arranged in sheets, in a hexagonal pattern like chicken wire, as shown in Figure 2.7. Graphite is a layered solid, in which the various planes are bonded by

Van der Waals forces. However, in its conventional form, graphite has an extremely low surface area (about  $0.5 \text{ m}^2 \text{ g}^{-1}$ ), and this aspect tends to limit its usefulness as a practical selective adsorption agent. So nano-structure graphite was synthesized in order to improve the hydrogen storage properties for practical uses (Miyaoaka *et al.*, 2006).

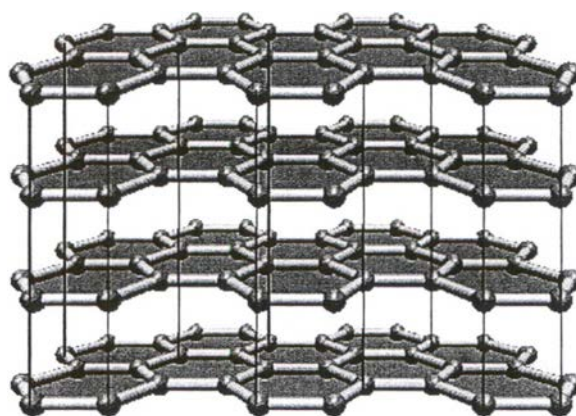


**Figure 2.7** Graphite structure

(<http://www.nano-enhanced-wholesale-technologies.com/faq/carbon-forms.htm>).

### (iii) Activated Carbon

Activated carbon is normally made by thermal decomposition of carbonaceous material followed by activation with steam or carbon dioxide at elevated temperatures. The structure of activated carbon consists of elementary microcrystallites of graphite, but these microcrystallites are stacked together in random orientation and it is the spaces between the crystals, which form the micropores. The graphite platelet structure gives activated carbon its very large surface and porosity, which allows it to adsorb a wide range of compounds.

### (iv) Metal-organic Frameworks (MOFs)

MOFs are a new class of crystalline materials consisting of metal ions linked together by organic ligands resulting in a highly microporous network. Owing to their high specific surface area and tailored pore dimensions, MOFs are ideal materials for hydrogen storage based on physisorption. Among all

classes of porous materials, MOFs show the highest specific surface area and hydrogen uptake at 77 K compared with carbon materials and zeolites (Hirscher and Panella, 2007)

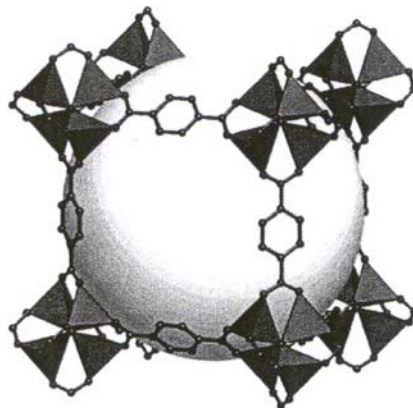
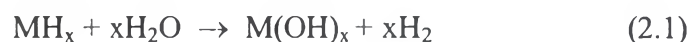


**Figure 2.8** Structure of MOF-5, IRMOF-8, for hydrogen storage (<http://www.public.asu.edu/~rosebudx/MOF-5N.jpg>).

#### 2.4.3.2 Chemical Hydrides ( $H_2O$ -reactive or Hydrolysis)

Chemical hydrogen storage is used to describe the storage technology, in which hydrogen is released via chemical reaction. Common reactions involve chemical hydrides with water or alcohol.

Hydrolysis is the reaction of a chemical hydride with water to liberate hydrogen gas. The reactions are as follows (Fakioglu *et al.*, 2004):



where M is a metal and x is its valence, or



where M is a Group I and X is a trivalent element from Group III.

The keys to react via hydrolysis are less violent reaction conditions for high stable metal hydrides as LiH, NaH, NaBH<sub>4</sub>, safety, and high

hydrogen liberated. Table 2.3 shows storage capacities of some light metal hydrides via hydrolysis (Schüth *et al.*, 2003). However, the materials are not reversible, and spent fuel or by-product is regenerated off-board. Therefore, large scale applications and high cost are issues for this reaction.

Up to now, Millennium Cell has developed  $\text{NaBH}_4$  for a practical use. In hydrolysis, Ru was added as a catalyst and by-product,  $\text{NaBO}_4$ , was regenerated back to  $\text{NaBH}_4$  by using coke or methane (Kojima and Haga, 2003).

**Table 2.3** Storage capacities of some light metal hydrides via hydrolysis (Schüth *et al.*, 2003)

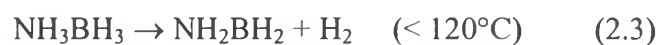
Hydride	Reaction	Capacity (wt %)
LiH	$\text{LiH} + \text{H}_2\text{O} \rightarrow \text{LiOH} + \text{H}_2$	7.7
$\text{LiBH}_4$	$\text{LiBH}_4 + 4\text{H}_2\text{O} \rightarrow \text{LiOH} + \text{H}_3\text{BO}_3 + 4\text{H}_2$	8.6
$\text{LiAlH}_4$	$\text{LiAlH}_4 + 4\text{H}_2\text{O} \rightarrow \text{LiOH} + \text{Al}(\text{OH})_3 + 4\text{H}_2$	7.3
NaH	$\text{NaH} + \text{H}_2\text{O} \rightarrow \text{NaOH} + \text{H}_2$	4.9
$\text{NaBH}_4$	$\text{NaBH}_4 + 4\text{H}_2\text{O} \rightarrow \text{NaOH} + \text{H}_3\text{BO}_3 + 4\text{H}_2$	7.3
$\text{NaAlH}_4$	$\text{NaAlH}_4 + 4\text{H}_2\text{O} \rightarrow \text{NaOH} + \text{Al}(\text{OH})_3 + 4\text{H}_2$	6.4
$\text{MgH}_2$	$\text{MgH}_2 + 2\text{H}_2\text{O} \rightarrow \text{Mg}(\text{OH})_2 + 2\text{H}_2$	6.3

#### 2.4.3.3 Chemical Hydrides (Thermal Decomposition)

The B-N-H compounds such as ammonia borane, guanidinium borohydride, and ethylene-diamine bisborane are interested for the chemical hydrogen storage due to their high theoretical hydrogen capacity (Sahler *et al.*, 2011). Moreover, in the B-N-H system, the corresponding protic and hydridic character of the hydrogen on the nitrogen and boron, respectively, allows a facile hydrogen elimination pathway, resulting in hydrogen release at low temperature (Wu *et al.*, 2008).

## (i) Ammonia Borane

Ammonia borane ( $\text{NH}_3\text{BH}_3$ ) is an attractive chemical hydrides because it contains 19.6 wt% hydrogen. The decomposition reactions with corresponding temperatures are provided in Eqs. (2.3)-(2.5). However, the reactions are not reversible, and off-board regeneration is required (Hirscher and Hirose, 2010).



## (ii) Guanidinium Borohydride

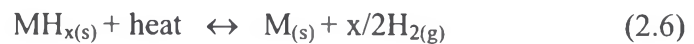
Guanidinium borohydride ( $(\text{N}_3\text{H}_6)\text{C}^+\text{BH}_4^-$ ) contains 10.7 wt% hydrogen, which also has potential as a hydrogen source. This material can be prepared by the ion exchange between  $\text{Ca}(\text{BH}_4)_2$  and guanidinium carbonate in water, and by the reaction between  $\text{NaBH}_4$  and guanidinium sulfate in isopropanol (Doroodian *et al.*, 2010). The decomposition takes place in two steps. The first step is a mixed evolution of hydrogen and ammonia, proceeding from about 90 to 150°C, while the second step (150-400°C) is dominated by the ammonia released (Tang *et al.*, 2011).

## 2.4.3.4 Rechargeable Metal Hydrides or Metal Hydrides

Hydrogen forms the metal hydrides with some metals and alloys leading to solid-state storage under moderate temperature and pressure that gives them the important safety advantage over the gas and liquid storage methods. Solid-state hydrides have higher hydrogen-storage density than hydrogen gas or liquid hydrogen. However, conventional materials appear inadequate for hydrogen storage due to their low gravimetric hydrogen uptake. Hence, there are several efforts

to reduce the hydrogen absorption/desorption temperature and also increase hydrogen storage capacities (Shi and Hwang, 2007).

Metal hydrides compose of metal atoms that constitute a host lattice and hydrogen atoms. The metal hydrides are a broad group of materials, which can undergo a reversible equilibrium reaction of the type:



where M is a metal and x is its valence. As written, the reaction is endothermic (heat absorbed) in the forward direction and exothermic (heat released) in the reverse direction.

Metal hydrides have the potential for reversible on-board hydrogen storage. Figure 2.9 shows the optimum operating P-T window for PEM fuel cell (see section 2.3) vehicular applications in the range of 1-10 atm and 25-120°C. However, issues with metal hydrides include low hydrogen capacity at the operating window, slow hydrogen uptake and release kinetics, and high cost of materials. According to Figure 2.9,  $\text{CaNi}_5\text{H}_4$ ,  $\text{NaAlH}_4$ , and  $\text{LaNi}_5\text{H}_6$  are potential metal hydrides for the PEM fuel cell operation.

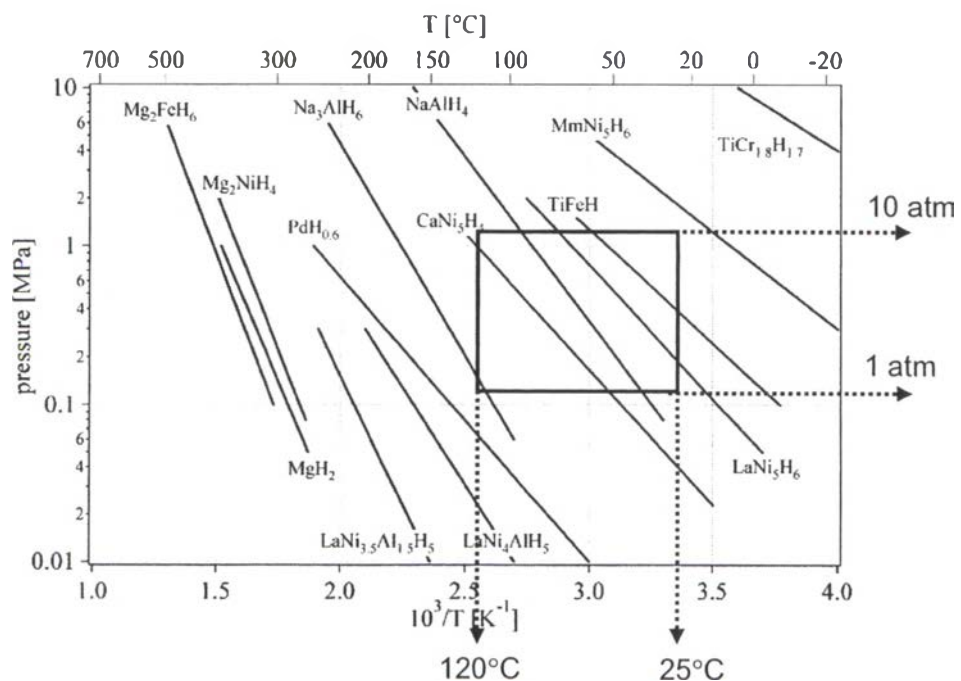


**Figure 2.9** Operating P-T window for PEM fuel cell (Sandrock and Huston, 1981).

## (i) Reaction Mechanism of Metal Hydride

The general mechanism of hydrogen absorption by a metal is shown in Figure 2.10. The hydrogen molecule is first weakly physisorbed on the surface and then dissociatively chemisorbed as strongly bound, individual H-atoms. The descriptions are hydrogen molecules dissociating at the surface of the absorbent into hydrogen atoms. These atoms then diffuse into the solid to form a hydride; two hydrogen atoms recombine during the desorption process to form H<sub>2</sub>. The host material initially dissolves some hydrogen as a solid solution ( $\alpha$ -phase); as the hydrogen pressure and concentration of hydrogen in the host increases, nucleation and growth of the hydride ( $\beta$ -phase) occurs (Züttel, 2004).

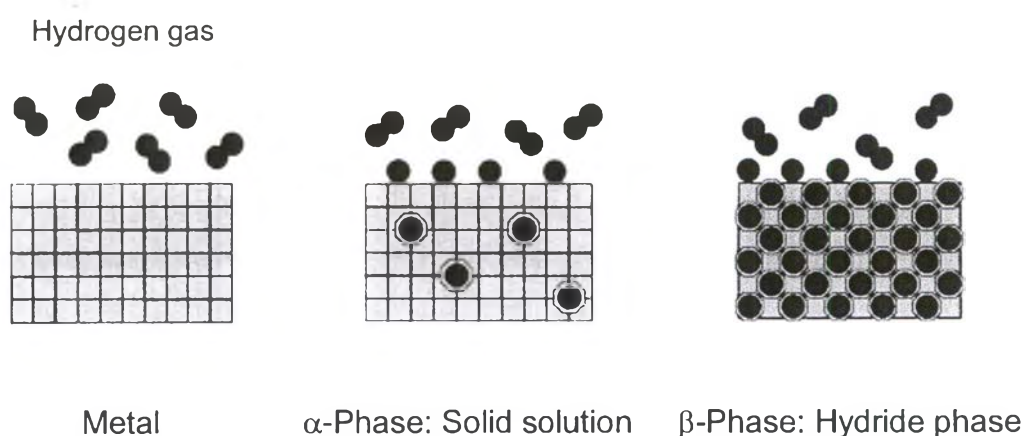


**Figure 2.10** Simplified absorption mechanism of the hydrogen into the metal hydrides, in  $\alpha$ -phase there is only some hydrogen adsorbed and in  $\beta$ -phase the hydride is fully formed (Züttel, 2004).

A schematic of phase transition is presented in Figure 2.11. When absorbing, hydrogen diffuses from the surface of the particle through the  $\beta$ -phase to the phase-transition interface and forms additional  $\beta$ -phase hydride. When desorbing, hydrogen from the phase-transition interface diffuses through the  $\alpha$ -phase to the surface of the particle where it is recombined into the form of molecular hydrogen (Chuang *et al.*, 2001).

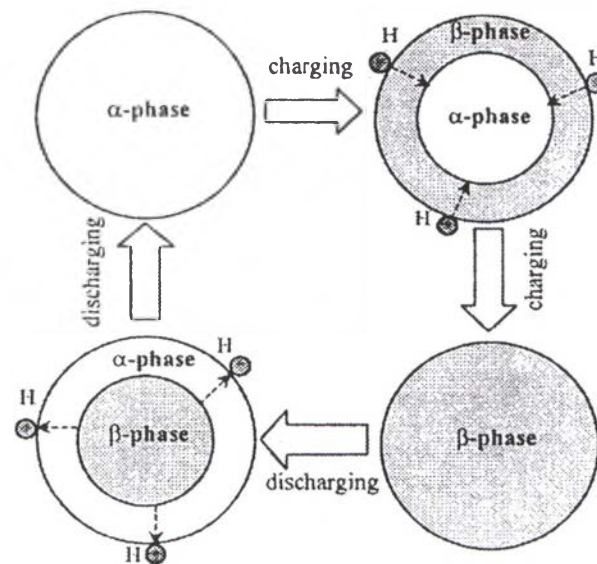


**Figure 2.11** Schematic of phase transition in metal hydride (Chuang *et al.*, 2001).

### (ii) Thermodynamic Aspects

The hydrogen formation from gaseous hydrogen is described by the pressure-composition isotherms, P-C isotherms, Figure 2.12. While the two phases of hydrogen,  $\alpha$  and  $\beta$ , coexist, the isotherms show a flat plateau, the length of which determines the amount of hydrogen that can be stored reversibly with small pressure variations. The two phase region ends at a critical point,  $T_c$ , after which the transition from  $\alpha$  to  $\beta$  is continuous (Züttel, 2004).

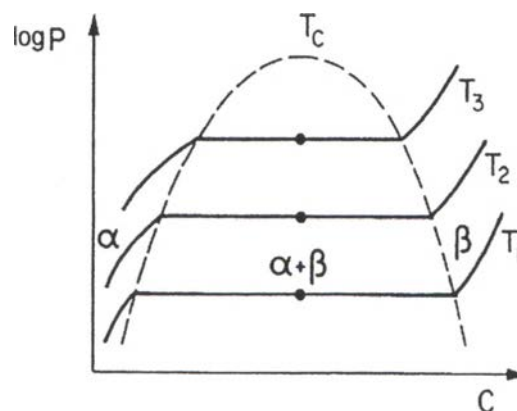


**Figure 2.12** Theoretical P-C isotherm of a metal hydride (Schlapbach, 1998).

The thermodynamic reaction equilibrium is defined with the equilibrium constant  $K$  (Hagström, 1999).

$$RT \ln K = \Delta H - T\Delta S \quad (2.7)$$

where  $\Delta H$  is the reaction enthalpy and  $\Delta S$  is the reaction entropy. For a solid-gas reaction, the equilibrium constant reduces to the pressure of the gas. Thus, the van't Hoff equation is obtained (Hagström, 1999).

$$\ln P = \frac{\Delta H}{RT} - \frac{\Delta S}{R} \quad (2.8)$$

The van't Hoff equation shows the plateau pressure is strongly dependent on temperature and is related to changes in enthalpy and entropy. Plotting of  $\ln P$  versus  $1/T$  gives the van't Hoff plot. The reaction enthalpy can be derived from the angular coefficient of the plot. The theoretical van't Hoff plot as shown in Figure 2.13 usually describes very well the real properties of metal hydrides and tells the suitability of P-T behaviors for practical uses (Sandrock, 1999).

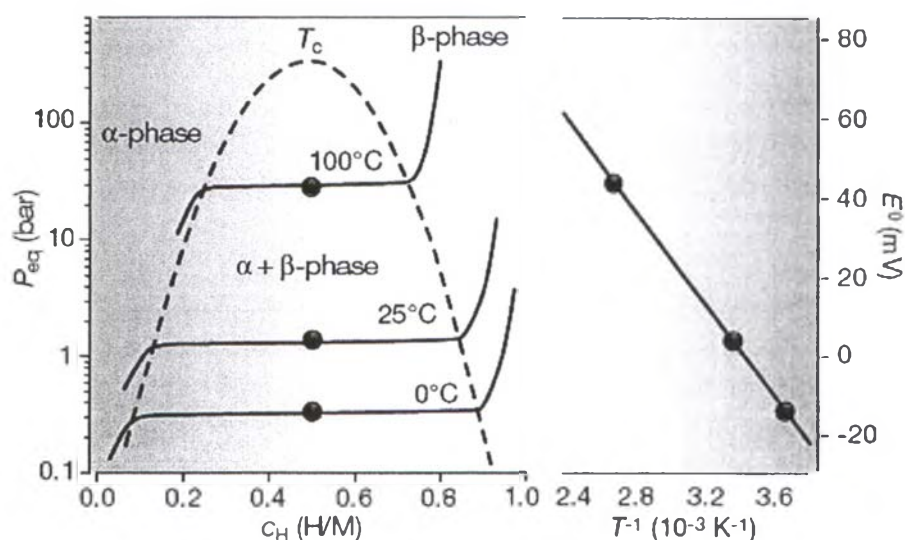


**Figure 2.13** Left: P-C isotherm, Right: The corresponding van't Hoff plot derived from the plateau pressures in the P-C isotherm (Schlapbach and Züttel, 2001).

(iii) The Activation Energy ( $E_A$ )

The activation energy is used to indicate the kinetic destabilization, which can be estimated by the Kissinger method (Kissinger, 1957) according to the following equation;

$$\ln \left[ \frac{\beta}{T_p^2} \right] = -\frac{E_A}{RT} + \ln \left[ \frac{k_0 R}{E_A} \right] \quad (2.9)$$

where  $\beta$  is the heating rate ( $\text{K}\cdot\text{min}^{-1}$ ),  $T_p$  is the peak temperatures (K),  $R$  is the gas constant ( $8.314 \text{ J (mol}\cdot\text{K)}^{-1}$ ) and  $k_0$  is the frequency factor. The activation energy is determined from the slope of the plot between  $\ln \left[ \frac{\beta}{T_p^2} \right]$  and  $\frac{1}{T_p}$  as shown in Figure 2.14 (Fan *et al.*, 2007). The activation energies were estimated to be  $156.75 \text{ kJ (mol H}_2\text{)}^{-1}$  for the  $\text{LiBH}_4$  and  $\text{MgH}_2$  mixture without  $\text{Nb}_2\text{O}_5$  (Figure 2.14(a)) and  $139.96 \text{ kJ (mol H}_2\text{)}^{-1}$  for the  $\text{LiBH}_4$  and  $\text{MgH}_2$  mixture doped with 16 wt%  $\text{Nb}_2\text{O}_5$  (Figure 2.14(b)).

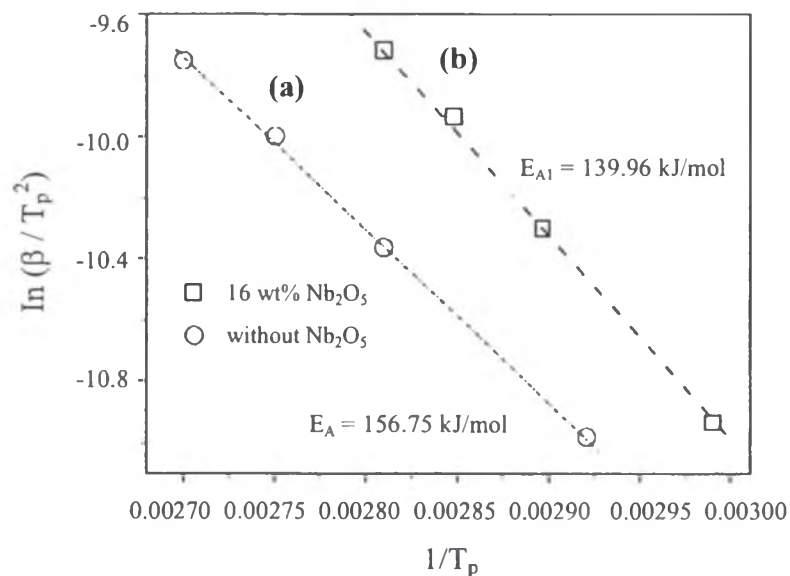


**Figure 2.14** The Kissinger plot (Fan *et al.*, 2007).

## 2.5 Metal Hydrides

Metal hydrides can be categorized into three major groups: simple metal hydrides, complex hydrides, and intermetallic compounds.

### 2.5.1 Simple Metal Hydrides

Storage of hydrogen in simple metal hydrides is possible since many metals react readily with hydrogen forming a stable metal hydride. For instance, magnesium, Mg, reacts with hydrogen forming a hydride of the form  $MgH_2$ . Mg is an excellent hydrogen storage medium because it can store about 7.7 wt% hydrogen. It is abundant and inexpensive. However, the main problems are the high binding energy of hydrogen in magnesium, since it desorbs hydrogen at the high temperature of 300°C 1 bar hydrogen. The absorption/desorption of hydrogen in magnesium is also very slow, and a catalyst is needed to accelerate the reaction (Sakintuna *et al.*, 2006).

### 2.5.2 Complex Hydrides

Complex hydrides have the potential for higher gravimetric hydrogen capacities than the simple metal hydrides. Elements from the Groups I, II, and III can form metal-hydrogen complexes, with a covalent or ionic bonding between metal and hydrogen. Typical complexes are tetrahedral with hydrogen on the corners, surrounding an Al or B atom, forming  $AlH_4^-$  or  $BH_4^-$  anions. The anions are compensated by cations, e.g., Li, Na or Mg, which are connected to the anions by sharing a hydrogen atom, e.g.  $NaAlH_4$  and  $LiBH_4$  (Züttel, 2004).

Complex hydrides containing Al or B complexes are called alanates and borohydrides, respectively. They are usually lightweighted with high gravimetric hydrogen densities, e.g.  $LiBH_4$ , with 18.4 wt %hydrogen. Because of their high gravimetric hydrogen densities, the complex hydrides could be ideal hydrogen storage materials for mobile applications. Unfortunately, they are also often very stable and decompose only at high temperatures, which sometimes are above their melting points (Züttel, 2004).

However, in 1996 Bogdanović and Schwickardi demonstrated reversible hydrogenation of  $\text{NaAlH}_4$ ,  $\text{Na}_3\text{AlH}_6$  and  $\text{Na}_2\text{LiAlH}_6$  at temperatures of  $180^\circ\text{C}$  and  $210^\circ\text{C}$ , by adding small amounts of Ti. Since then, an intensive research on alanates and borohydrides has been made.

### 2.5.3 Intermetallic Compounds

Intermetallic compounds are more like solid solutions, and hydride complexes that are formed with transition metals. There are several types of intermetallic compounds containing different amounts of A (strong elements) and B (weak elements) elements are discussed below.

*AB<sub>5</sub> Intermetallic Compounds* The most important example of  $\text{AB}_5$  class alloys is  $\text{LaNi}_5$ . The family has an extraordinary versatility because many different elemental species can be substituted into A and B lattice sites. Usual examples of substitutes for A are Mm, Ca, Y, Zr. and for B are Al, Mn, Si, Zn, Cr, Fe, Cu, and Co (Beltowska-Brzezinska *et al.*, 2001). A partial replacement of the A and B components significantly changes the alloy macrostructure. The hydrogen capacity of  $\text{AB}_5$  hydrides is unfortunately low and the cost is quite high (Sandrock, 1999).

*AB<sub>2</sub> Intermetallic Compounds* The  $\text{AB}_2$  alloys represent a large and versatile group with favorable PCT properties near the ambient temperature. The A elements are usually Ti, Zr, Hf, or a lanthanide. The B elements can be a variety of transition and non-transition metals, such as V, Cr, Mn, and Fe. Hydrogen capacities of  $\text{AB}_2$  alloys are comparable to  $\text{AB}_5$  on a reversible basis generally have higher maximum capacities, 1.5-2 wt% (Jang *et al.*, 1999).

*AB Intermetallic Compounds* The AB alloys are mainly TiFe-based. They tend to have two plateaus, the upper of which not necessarily very stable, and the hysteresis is also quite large. PCT properties can be modified by partial substitution of Fe by Mn or Ni (Sandrock, 1999). The maximum hydrogen capacities vary from < 1 to 2 wt% (<http://hydpark.ca.sandia.gov>).

Other intermetallic compounds include  $\text{A}_2\text{B}$ ,  $\text{AB}_3$ ,  $\text{A}_2\text{B}_7$ ,  $\text{A}_3\text{B}$ , etc. None of which has attained commercial interest although some of these have good hydrogen capacities but do not have favorable PCT properties.

## 2.6 Modification of Lithium Borohydride

### 2.6.1 Hydrogen Storage Properties of Lithium Borohydride

Lithium borohydride or lithium tetrahydroboride,  $\text{LiBH}_4$  is considered as extremely high hydrogen content, 18.4 wt%. However, it is not established for on-board applications due to too high desorption temperature. The reaction as follows:



As in Eq. (2.10),  $\text{LiBH}_4$ , melting point is  $275^\circ\text{C}$  (Schlesinger and Brown, 1940). Theoretically, its desorption is limited to 13.5 wt% hydrogen due to formation of  $\text{LiH}$ .

The first report of  $\text{LiBH}_4$  appeared in 1940 by Schlesinger and Brown who synthesized  $\text{LiBH}_4$  by the reaction of ethyllithium with diborane at  $550\text{-}700^\circ\text{C}$  and 30-150 bar hydrogen.

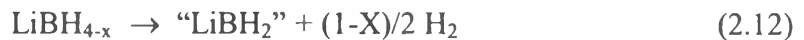
Fedneva *et al.* (1964) studied the desorption of  $\text{LiBH}_4$  by means of thermal analysis (DTA). The results reported three peaks; the first peak at  $108\text{-}112^\circ\text{C}$  corresponds to polymorphic transformation. The second peak at  $268\text{-}286^\circ\text{C}$  shows the release of 2 wt% hydrogen in  $\text{LiBH}_4$  due to the fusion, and the small effects from the last peak at  $483\text{-}492^\circ\text{C}$ .

The amount of actual desorbed hydrogen significantly depends on temperature and catalyst as reported by Züttel *et al.* (2003a,b). Result of pure  $\text{LiBH}_4$  shows that hydrogen desorption starts at a temperature range from  $320\text{-}600^\circ\text{C}$  with the total amount hydrogen at 9 wt%. After that,  $\text{SiO}_2$ -powder was added to  $\text{LiBH}_4$  in order to destabilize the interstitial hydrogen atoms. The decomposition reaction started at lower temperatures from  $200\text{-}500^\circ\text{C}$  and the total hydrogen desorption was 13.5 wt%. The hydrogen desorption mechanism of  $\text{SiO}_2$  catalyzed  $\text{LiBH}_4$  were three steps as follows:

1. Structure transition at  $T = 108^\circ\text{C}$ :



2. First hydrogen peak starting at  $T = 200^\circ\text{C}$ :



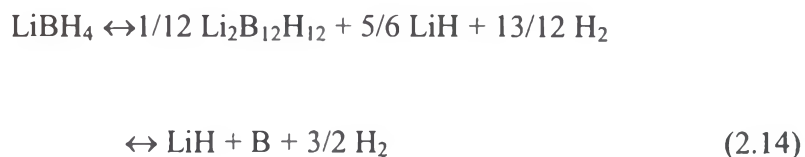
3. Second hydrogen peak starting at  $T = 453^\circ\text{C}$ :



where “LiBH<sub>2</sub>” is the partial decomposed LiBH<sub>4</sub>.

Mauron *et al.* (2008) further studied the stability and reversibility of LiBH<sub>4</sub> by pressure-concentration-temperature measurements under constant hydrogen flows and extrapolated to equilibrium. According to the van't Hoff equation, enthalpy of reaction  $\Delta_r H = 74 \text{ kJ (mol of H}_2\text{)}^{-1}$  and entropy of reaction  $\Delta_r S = 115 \text{ J (K. mol of H}_2\text{)}^{-1}$ . It is shown that the reaction could be reversed at a temperature of  $600^\circ\text{C}$  and at a pressure of 15.5 MPa. The formation of LiBH<sub>4</sub> was confirmed by X-ray diffraction. In the rehydrided material 8.3 wt% hydrogen was desorbed in a temperature-programmed desorption measurement compared to 10.9 wt% desorbed in the first dehydrogenation.

Ohba *et al.* (2006) reported that LiBH<sub>4</sub> could decompose via Li<sub>2</sub>B<sub>12</sub>H<sub>12</sub> intermediate compound. They studied by using the first-principles calculation. The proposed decomposition reaction of LiBH<sub>4</sub> via this intermediate compound is shown in Eq. (2.14). The hydrogen content and enthalpy of the first reaction were estimated to be 10 wt% and  $56 \text{ kJ (mol of H}_2\text{)}^{-1}$ , respectively, and those of the second reaction were 4 wt% and  $125 \text{ kJ (mol of H}_2\text{)}^{-1}$ .



However,  $\text{LiBH}_4$  is too stable for on-board applications but the high hydrogen content is a trade-off. According to the report of Vajo and Olson (2007), the thermodynamic constraints can be improved by (1) the formation of a new single-phase due to an atomic substitution or alloying and (2) the combinations of binary and complex hydrides to form new compounds. For the reaction kinetics, the two methods were (1) addition of catalysts and (2) reduction particle size of metal hydrides.

#### 2.6.2 Destabilization of Lithium Borohydride by Adding Additive/Catalyst

Au *et al.* (2008) reported the use of various metal oxides and metal chlorides to modify lithium borohydride for reversible hydrogen storage. For the oxide-modified borohydride, 75%  $\text{LiBH}_4$  + 25%  $\text{TiO}_2$ , desorbed 9 wt% hydrogen from 100 to 600°C and absorbed 8 wt% hydrogen at 600°C and 0.7 MPa. The chloride-modified borohydride,  $\text{LiBH}_4$  + 0.2 $\text{MgCl}_2$  + 0.1 $\text{TiCl}_3$ , desorbed 5 wt % hydrogen from 60 to 450°C and absorbed 4.5 wt% hydrogen at 600°C and 70 bar. The residual gas analyzer (RGA) spectra showed no diborane evolved from the above materials during dehydrogenation. The reversibility of oxide-modified  $\text{LiBH}_4$  deteriorated during repeatedly dehydrogenating–rehydrogenating due to increasing formation of  $\text{Li}_3\text{BO}_3$  and sequent deficiency of boron and lithium.

Fang *et al.* (2008) studied  $\text{LiBH}_4$  incorporated into an activated carbon scaffold using a chemical impregnation method. The  $\text{LiBH}_4/\text{AC}$  sample started to release hydrogen from just 220°C, which is 150°C lower than of  $\text{LiBH}_4$ . The dehydrogenation rate of the  $\text{LiBH}_4/\text{AC}$  sample was also faster than that of  $\text{LiBH}_4$ .

Mosegaard *et al.* (2008) investigated the interaction between  $\text{LiBH}_4$  and the additives ( $\text{SiO}_2$ ,  $\text{TiCl}_3$ ,  $\text{LiCl}$ , and Au). It was found that  $\text{SiO}_2$  reacted with molten  $\text{LiBH}_4$  could form  $\text{Li}_2\text{SiO}_3$  or  $\text{Li}_4\text{SiO}_4$  depending on amounts of  $\text{SiO}_2$ . A solid-state reaction between  $\text{LiBH}_4$  and  $\text{TiCl}_3$  formed  $\text{LiCl}$  at the room temperature.

Au was found to react with molten  $\text{LiBH}_4$  and form a Li-Au alloy with  $\text{CuAu}_3$ -type structure.

Zhang *et al.* (2008) doped  $\text{SiO}_2$ - $\text{LiBH}_4$  with  $\text{TiF}_3$  to avoid the formation of  $\text{Li}_4\text{SiO}_4$  and enhance the reversible hydrogen storage. For  $\text{LiBH}_4$ -20 wt%  $\text{SiO}_2$ -30 wt%  $\text{TiF}_3$  composite, the dehydrogenation temperature started from  $70^\circ\text{C}$  and decreased by an average of  $100^\circ\text{C}$  from that of  $\text{LiBH}_4$ -20 wt%  $\text{SiO}_2$ . Its maximum amount attained 8.3 wt% below  $500^\circ\text{C}$ . Doped  $\text{TiF}_3$  noticeably reduces the energy activation of the reaction at interface. The hydrogen absorption under the pressure of 4.5 MPa is temperature dependent and reached 4 wt % hydrogen within 14,000 sec at  $500^\circ\text{C}$ .

Cahen *et al.* (2009) reported that the  $\text{LiBH}_4$ /carbon composite with a 33:67 weight ratio released hydrogen 3.4 wt% at  $300^\circ\text{C}$  with a fast reaction kinetics (90 min). Characterizations by DSC and TDS showed that the decomposition of composite occurred in one step immediately above the melting temperature of  $\text{LiBH}_4$  ( $280^\circ\text{C}$ ) without the formation of intermediate compounds as found in the neat  $\text{LiBH}_4$ . The carbonaceous matrix may improve the heat transfer associated with the endothermic character of the  $\text{LiBH}_4$  decomposition.

Wellons *et al.* (2009) enhanced the hydrogen storage properties of  $\text{LiBH}_4$  by adding fullerene. They reported that the fullerene not only lowered hydrogen desorption temperature but also absorbed hydrogen at a low temperature of  $350^\circ\text{C}$ . The lower of cycling capacity was probably due to the formation of diboranes or other irreversible intermediates.

Xia *et al.* (2009) studied the hydrogen storage properties of  $\text{LiBH}_4$  ball milled with various ratios of Ni powders. It was found that Ni improved the dehydrogenation of  $\text{LiBH}_4$  by releasing hydrogen below  $600^\circ\text{C}$ . From the van't Hoff equation, the desorption enthalpy of  $\text{LiBH}_4$ -Ni system was  $\Delta H = -60.76 \text{ kJ mol}^{-1} \text{ H}_2$ , which is similar to that of the pure  $\text{LiBH}_4$ . Pressure-composition-temperature revealed that Ni accelerated the dehydrogenation rate of  $\text{LiBH}_4$ . Furthermore, the  $\text{LiBH}_4$ -Ni system could be reversed partly at  $600^\circ\text{C}$  and 10 MPa hydrogen.

Yu *et al.* (2009) investigated the dehydrogenation of  $\text{LiBH}_4$  ball-milled with hydrogenated 40Ti-15Mn-15Cr-30V alloy. It was found that there was

a mutual catalysis between the two hydrides, lowering the temperature of hydrogen release from both hydrides. In the case of 1 h milled LiBH<sub>4</sub>/40Ti–15Mn–15Cr–30V with a mass ratio of 1:4, the peak temperatures of 40Ti–15Mn–15Cr–30V and LiBH<sub>4</sub> were decreased to 195 and 390°C, respectively, which were 77 and 50°C lower than the respective hydride on its own.

Fang *et al.* (2010) added a carbon material (graphite, purified single-walled carbon nanotube, and activated carbon) to LiBH<sub>4</sub>. It was found that all the carbon additives can improve the kinetics and hydrogen capacity of LiBH<sub>4</sub>. The promoting effect of the carbon additives was largely attributed to their heterogeneous nucleation and micro-confinement effect on the reversible dehydrogenation of LiBH<sub>4</sub>.

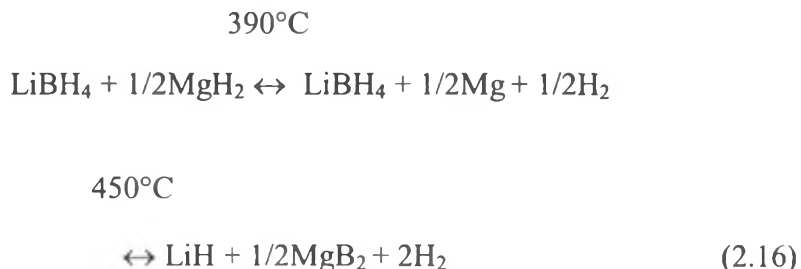
### 2.6.3 Destabilization of Lithium Borohydride by Reacting with Magnesium Hydride

Vajo *et al.* (2005) were the first research group who reported the work on thermodynamic destabilization by the combinations of LiH and MgB<sub>2</sub> (2:1 mole ratio). The theoretical reaction mechanism was shown;



The maximum hydrogen capacity was 11.4 wt%. They found that the hydrogen desorption/absorption enthalpy was lowered by 25 kJ (mol of H<sub>2</sub>)<sup>-1</sup> as compared with LiBH<sub>4</sub>. The possible reason might be the formation of MgB<sub>2</sub> upon hydrogen desorption. A predicted equilibrium pressure of 1 bar was approximately at 225°C.

A few years later, Bösenberg *et al.* (2007) analyzed the reaction mechanism of the reactive hydride composite using high-pressure differential scanning calorimetry measurements and in situ synchrotron powder X-ray diffraction measurements. They found that the hydrogen desorption followed in two steps;



However, Nakagawa *et al.* (2007) found that the hydrogen desorption condition affected the desorbed products of the LiBH<sub>4</sub> and MgH<sub>2</sub> mixture. Under 0.5 MPa hydrogen, The products after hydrogen desorption at a temperature above 400°C were MgB<sub>2</sub>, LiH, and H<sub>2</sub>, whereas under an inert gas, the hydrogen desorption products were transformed into Mg, B, LiH, and H<sub>2</sub> in a temperature range from 350 to 430°C. It was resulted from the molten LiBH<sub>4</sub> did not decompose into LiH, B, and H<sub>2</sub> below 450°C under 1 MPa hydrogen, while the LiBH<sub>4</sub> decomposed even below 450°C under an inert gas atmosphere.

Pinkerton *et al.* (2007) extended the work of Vajo *et al.* (2005) by establishing the hydrogen pressure-temperature phase diagram for the TiCl<sub>3</sub> catalyzed LiBH<sub>4</sub> and MgH<sub>2</sub> mixture. They reported that, at an elevated temperature, the formation of MgB<sub>2</sub> was thermodynamically favored for the LiBH<sub>4</sub> and MgH<sub>2</sub> mixture. However, at a low hydrogen pressure and high temperature, LiH, which decomposed from LiBH<sub>4</sub>, recombined with amorphous boron at very poor kinetics resulting in the system did not fully rehydrogenate. But applying an hydrogen gas overpressure at least 0.3 MPa during hydrogen desorption, suppressed direct decomposition of LiBH<sub>4</sub> and reaction of Mg with LiBH<sub>4</sub> produced LiH and MgB<sub>2</sub>, which was fully reversible.

In the case of destabilization of LiBH<sub>4</sub> and MgH<sub>2</sub> mixture by adding a catalyst, a number of research works have been reported. For example, Vajo and Olson (2007) added 2-3 mol% TiCl<sub>3</sub> to the mixture of LiH and MgB<sub>2</sub>. They found that 8-10 wt% hydrogen can reversibly be stored at 315-400 °C.

Bösenberg *et al.* (2007) doped the LiBH<sub>4</sub> and MgH<sub>2</sub> mixture with different oxides, borides, chlorides and metal-organic compounds. They found that only a few samples doped with 5 at% of VCl<sub>3</sub>, titanium isopropoxide, and SiO<sub>2</sub> can

lower the hydrogen desorption temperature as compared to the non-catalysed material.

Fan *et al.* (2008) studied  $\text{LiBH}_4/\text{MgH}_2$  (mass ratio 1:2) doped with 16 wt%  $\text{Nb}_2\text{O}_5$  composite. The results showed that the maximum hydrogen capacity of 6–8 wt% released at below 400°C for hydrogen desorption and that of 5–6 wt% released at 400°C under 1.9 MPa hydrogen for hydrogen absorption. The destabilization of the  $\text{LiBH}_4$  and  $\text{MgH}_2$  mixture was from the formation of an intermediate compound,  $\text{NbH}_2$  and  $\text{MgB}_2$ , in the milling process. The lower of the activation energies by Kissinger method confirmed the benefit of  $\text{Nb}_2\text{O}_5$ .

Mao *et al.* (2007) found that the hydrogen storage properties of  $\text{LiBH}_4/\text{Mg}$  mixtures exhibited a dramatic improvement as compared to plain Mg. For example, at 250°C, a  $\text{LiBH}_4/\text{Mg}$  (mass ratio 1:4) composite absorbed 6.7 wt% hydrogen in 60 min, while only less than 1 wt% hydrogen was absorbed by Mg in the same period under similar conditions. Furthermore, highly activated  $\text{MgH}_2$  was synthesized by ball milling  $\text{LiBH}_4/\text{Mg}$  mixtures under high hydrogen pressure. It exhibited superior kinetics by absorbing 5.78 wt% hydrogen at 200°C within 100 min.

Wang *et al.* (2008) showed that  $\text{TiF}_3$  highly promoted the dehydrogenation reaction in the Li–Mg–B–H system. Compared to  $2\text{LiH} + \text{MgB}_2$  sample, the  $2\text{LiH} + \text{MgB}_2 + 0.01\text{TiF}_3$  sample exhibited significantly reduced dehydrogenation temperature and markedly enhanced dehydriding rate. Furthermore, the catalytic enhancement arising upon adding  $\text{TiF}_3$  additive was observed to persist well in the hydrogenation/dehydrogenation cycles.

Wan *et al.* (2008) was the first group who synthesized nanoscale  $\text{LiBH}_4$  and  $\text{MgH}_2$  mixture in order to obtain the hydrogen desorption temperature lower than the melting point of  $\text{LiBH}_4$  by high energy ball milling at 600 rpm with a 60:1 ball-to-powder ratio under an ultrahigh-purity argon atmosphere, and the milling temperature was maintained at 20°C. The achieved milling time was 120 min. They found that up to 8.3 wt% hydrogen uptake can be obtained without any catalyst.

Du *et al.* (2009) reported the *ab initio* density functional theory results from the hydrogenation of  $\text{MgB}_2$ . They found that the activation barrier for the dissociation of hydrogen were 0.49 and 0.58 eV for the B and Mg-terminated  $\text{MgB}_2$  (0001) surface, respectively. This implied that the dissociation kinetics of hydrogen on a  $\text{MgB}_2$  (0001) surface should be greatly improved compared to that in pure Mg materials.

Puszekiel and Gennari (2009) produced composite powders of  $\text{Mg}_{50}\text{Ni}$  and  $\text{Mg}_{15}\text{Fe}$  with  $\text{LiBH}_4$  by short-time milling under an argon atmosphere. The composites enhanced the reversible hydrogen capacities of 7 wt% for Ni and 5.5 wt% for Fe at  $300^\circ\text{C}$ . The presence of  $\text{LiBH}_4$  did not modify the thermodynamic, but did improve the reaction kinetic of the composites.

Deprez *et al.* (2010) reported the  $\text{LiBH}_4/\text{MgH}_2$  mixture with and without the Ti-iso additive. They found that a small additive nanoparticles was the main factor improving desorption and absorption kinetics by favoring heterogeneous nucleation of  $\text{MgB}_2$ , resulting in its grain refinement. The higher number of nucleation sites in the presence of the additive produced a decrease in the crystallite size in a factor of 50% for the  $\text{MgB}_2$  and LiH phases during desorption. In addition, the reduction in crystallite size during the milling process of the  $\text{LiBH}_4$  and  $\text{MgH}_2$  phases was lost after the first cycle.

Wang *et al.* (2010) investigated the hydrogen storage behaviors of  $\text{LiBH}_4$  and  $\text{MgH}_2$  mixture doped with various carbons. Among the carbon additives, purified single-walled carbon nanotubes exhibited the most prominent effect on the kinetic improvement and cyclic stability of the mixture. They released almost 10 wt% hydrogen within 20 min at  $450^\circ\text{C}$ , which was about two times faster than that of the undoped mixture.

Price *et al.* (2010) demonstrated the influence of stoichiometry in the cycling kinetics under different decomposition conditions.  $2\text{LiBD}_4:\text{MgD}_2$  and  $0.3\text{LiBD}_4:\text{MgD}_2$  desorbed under 1 bar deuterium and dynamic vacuum and absorbed under 100 bar  $\text{D}_2$  at  $400^\circ\text{C}$ . The hydrogen uptake was investigated through the formation of deuterided products. The results reported that the 0.3:1 sample had 90% deuteriding occurring within 10 min, while the 2:1 sample showed only 60% deuteriding after 4 h under similar conditions.

Bösenberg *et al.* (2010) investigated the decomposition pathway of LiBH<sub>4</sub>-MgH<sub>2</sub> reactive hydride composites as a function of pressure and temperature. Individual decomposition of MgH<sub>2</sub> and LiBH<sub>4</sub> was observed at 450 °C and 3 bar H<sub>2</sub>, whereas simultaneous desorption of H<sub>2</sub> from LiBH<sub>4</sub> and formation of MgB<sub>2</sub> was observed at 400 °C and 0.5 MPa hydrogen. The simultaneous desorption of hydrogen from LiBH<sub>4</sub> and MgH<sub>2</sub> without intermediate formation of metallic Mg could not be observed.

Shaw *et al.* (2010) studied the solid-state hydriding mechanism of 2LiH + MgB<sub>2</sub> mixtures. It was found that the solid-state hydriding proceeds in two elementary steps. The first step was the ion exchange between the Mg<sup>2+</sup> and Li<sup>+</sup> ions in the MgB<sub>2</sub> crystal to form an intermediate compound (Mg<sub>1-x</sub>Li<sub>2x</sub>)B<sub>2</sub>. The second step was the continuous ion exchange and simultaneous hydrogenation of (Mg<sub>1-x</sub>Li<sub>2x</sub>)B<sub>2</sub> to form LiBH<sub>4</sub> and MgH<sub>2</sub>. This finding was consistent with the observed diffusion-controlled hydriding kinetics.

Zeng *et al.* (2010) found an “H-D” exchange between MgD<sub>2</sub> and LiBH<sub>4</sub> during heating and this exchange proceeded even in solid phases. The hydrogen desorption temperature of the first step was over 300°C, even though catalyst-doped MgH<sub>2</sub> released hydrogen at 200°C. The above results suggested the hydrogen desorption from catalyst-doped MgH<sub>2</sub> was somehow suppressed by the hydrogen exchange effect between MgH<sub>2</sub> and LiBH<sub>4</sub>.

Fernández *et al.* (2011) compared the behaviour of the Nb- and Ti-based additives in MgH<sub>2</sub> and MgH<sub>2</sub> + 2LiBH<sub>4</sub>. They found that the Nb additive performed its activity at the surface, while the Ti additive migrated to the bulk. The Nb additive facilitated the diffusion of hydrogen through the diffusion barriers both in desorption and absorption. The Ti additive enhanced the heterogeneous nucleation of MgB<sub>2</sub> during desorption and producing a distinct grain refinement that favours both sorption kinetics.

Liu *et al.* (2011) applied three Ce-based additives to improve the hydrogen storage performance of LiBH<sub>4</sub> + 1/2MgH<sub>2</sub> composites. The composites with Ce additives demonstrated significantly improved dehydrogenation kinetics and cyclic stability compared with the pure composite. The CeB<sub>6</sub> formed in the composite may act as the nucleus for MgB<sub>2</sub> formation during dehydrogenation.

Mao *et al.* (2011) investigated effects of ruthenium nanoparticles supported on multiwalled carbon nanotubes (Ru/C) on the hydrogen sorption properties of  $\text{LiBH}_4\text{-MgH}_2$  systems. The experimental results showed that the Ru/C catalyst could reduce the dehydrogenation temperature, enhance the dehydrogenation kinetics, and dramatically improve the reversible capacity under moderate conditions.

Wang *et al.* (2011) improved the hydrogen desorption properties of  $\text{LiBH}_4$  by adding  $\text{MgH}_2$  and  $\text{NdCl}_3$ . The results showed that adding either  $\text{NdCl}_3$  or  $\text{MgH}_2$  alone could not promote the decomposition of  $\text{LiBH}_4$ . But for the  $\text{NdCl}_3$  doped  $\text{LiBH}_4\text{-MgH}_2$  composites, both decomposition rate and capacity of  $\text{LiBH}_4$  were greatly enhanced. The  $\text{NdH}_2$  phase resulting from reaction between  $\text{MgH}_2$  and  $\text{NdCl}_3$  might be responsible for the enhanced decomposition of  $\text{LiBH}_4$ .

Xia *et al.* (2011) studied effects of  $\text{MoCl}_3$  on the hydrogen desorption and absorption properties of  $\text{LiBH}_4$  and  $\text{MgH}_2$  mixture. The reversible hydrogen capacity was about 7 wt% hydrogen at  $300^\circ\text{C}$ . The formation of metallic Mo resulted in the improvement of desorption and absorption performance. The activation energy of the mixture with  $\text{MoCl}_3$  was  $43 \text{ kJ (mol of H}_2\text{)}^{-1}$ , which was lower than that of the pure mixture about  $10 \text{ kJ (mol of H}_2\text{)}^{-1}$ . This result confirmed the activity of Mo.

Yang *et al.* (2011) reported the effect of addition of  $\text{F}^-/\text{Cl}^-$  containing dopants (viz.  $\text{LiBF}_4$ ,  $\text{NH}_4\text{F}$ ,  $\text{LiAlCl}_4$  and  $\text{NH}_4\text{Cl}$ ) on the hydrogen released from  $2\text{LiBH}_4\text{:1MgH}_2$  and  $\text{LiBF}_4$  was found to be the most effective among the dopants studied.  $2\text{LiBH}_4\text{:1MgH}_2$  doped with both  $\text{LiBF}_4$  and  $\text{NbF}_5$  catalyst was found to reduce the hydrogen desorption temperature as compared with  $\text{LiBH}_4$  and  $\text{MgH}_2$  by  $55$  and  $112^\circ\text{C}$ , respectively. This sample partially absorbed hydrogen under and 100 bar  $400^\circ\text{C}$ .